AIAA JOURNAL
Vol. 33, No. 7, July 1995

Interacting Loads in an Orthogonally Stiffened Composite Cylindrical Shell

Eric R. Johnson* and Naveen Rastogi†
Virginia Polytechnic Institute and State University, Blacksburg, Virginia 24061-0203

The distributions of the interacting loads between orthogonal stiffeners and the shell wall are computed for a long circular cylindrical shell subjected to internal pressure. Identical stringers are equally spaced around the circumference, and identical frames, or rings, are equally spaced along the length. Both the stringers and frames are on the inside of the shell wall. Closed-end pressure vessel effects are included. A comparison is made between linear elastic response and geometrically nonlinear elastic response. The example problem has dimensions of the fuselage of a typical transport aircraft and has a composite material shell wall and symmetric stiffeners. The inclusion of geometric nonlinearity is found to increase the loads carried by the stiffeners and to decrease the pillowing, or bending, of the shell. However, the nonlinear response exhibits the most severe bending in a narrow boundary layer adjacent to the stringer midway between the frames, resulting in a larger transverse shear resultant in the shell compared with the linear response. The interacting normal load intensity exhibits singular behavior at the stiffener intersection for both linear and nonlinear analyses.

Introduction

THE cabin pressurization in a transport aircraft causes about a 10-psi pressure differential across the skin. An unstiffened or a monocoque fuselage would carry this internal pressure load as a shell in membrane response, like a pressure vessel. However, internal longitudinal and transverse stiffeners are necessary to carry loads due to flight maneuvers, landing, and ground handling, etc. How the loads are transferred in the stiffener-to-skin joints under pressurization is necessary for determining the load capacity of these joints. In particular, a local concentration of the interacting loads between the stiffeners and the skin occurs at the stiffener intersection, as will be shown in the sequel. Also, the presence of the internal stiffeners prevents the fuselage skin from expanding as a membrane, and the skin bulges, or "pillows," between the stiffeners under the action of internal pressure. Where the skin is restrained against expansion as a membrane along the stiffeners, a localized bending boundary layer is formed that causes a concentration of stress.

The design of stiffener-to-skin joints was cited in Ref. 1 as one of the major technological issues in utilizing graphite/epoxy composites in the fuselage of a large transport aircraft. Stiffeners can be attached to the skin by either fasteners, cocuring, adhesive bonding, or some combination of these methods. In general, adhesive joints are more efficient for lightly loaded joints, and mechanically fastened joints are more efficient for heavily loaded joints.[2] Where fasteners are required in a graphite/epoxy structure, aluminium fasteners cannot be used because of galvanic corrosion to the metal. More expensive fasteners, like titanium, are required to avoid corrosion.

The objective of this paper is to develop an analysis of an orthogonally stiffened composite cylindrical shell subjected to internal pressure. This analysis is used to study the distribution of the interacting loads between the shell and stiffeners and to study the pillowing of the shell, for a geometry and pressure typical of a large transport aircraft. Both a linear elastic response and a geometrically nonlinear elastic response are considered and compared. Besides the results presented in this paper, the intent is to develop an analysis/design capability that could be used for the design of the stiffener-to-skin joint and the design of the laminated wall construction for the skin. A potential benefit of such an analysis/design capability is to use fewer expensive fasteners in the graphite/epoxy fuselage.

Presented as Paper 94-1646 at the AIAA/ASME/ASCE/AHS/ASC 35th Structures, Structural Dynamics, and Materials Conference, Hilton Head, SC, April 18–20, 1994; received July 25, 1994; revision received Nov. 5, 1994; accepted for publication Nov. 7, 1994.

*Professor, Department of Aerospace and Ocean Engineering. Senior Member AIAA.

†Graduate Research Assistant, Department of Aerospace and Ocean Engineering. Student Member AIAA.

Mathematical Model

An idealized mathematical model is assumed for the semimonocoque fuselage to study the generic characteristics of the response in the vicinity of the stiffeners' intersection. The model is of a very long circular cylindrical shell internally stiffened by identical stringers equally spaced around the circumference and identical frames, or rings, equally spaced along the length. In general, the spacing of the stringers is not the same as that of the rings. The structure is periodic both longitudinally and circumferentially, and the loading is spatially uniform. Consequently, a structural repeating unit can be defined whose deformation determines the deformation of the entire structure. A typical repeating unit consists of a portion of the shell wall centered over the portions of stringer and ring as shown in Fig. 1. The radius of the middle surface of the undeformed cylindrical shell is denoted by R, and the thickness of the shell is denoted by t. Axial coordinate x and the circumferential angle θ are lines of curvature on the middle surface, and the thickness coordinate is denoted by ζ, with $-t/2 \leq \zeta \leq t/2$. The origin of the surface coordinates is centered over the stiffeners' intersection so that $-l \leq x \leq l$ and $-\Theta \leq \theta \leq \Theta$, where $2l$ is the axial length, and $2R\Theta$ is the circumferential arc length of the repeating unit.

The stiffeners are mathematically modeled as one-dimensional elements, or discrete beams, so that the actions transmitted by the stiffeners to the inside of the shell wall are represented by distributed line load intensities. In this paper it is assumed that the stringer is symmetric about the $x-\zeta$ plane through its centroidal axis, and the ring is symmetric about the $\theta-\zeta$ plane through its circular reference axis. On the basis of the symmetry about the x and θ axes for the unit, only the interacting line load components tangent and normal to the stiffeners are included in the analysis. The interacting line load intensities per unit undeformed length along the contact lines are denoted by $\lambda_{xs}(x)$ for the component tangent to the stringer, $\lambda_{\zeta s}(x)$ for the component normal to the stringer, $\lambda_{\theta r}(\theta)$ for the component tangent to the ring, and $\lambda_{\zeta r}(\theta)$ for the component normal to the ring. These interacting loads acting in a positive sense on the inside surface of the shell are shown in Fig. 2. The purpose of the analysis is to determine these distributed line loads.

An enclosed volume to contain the pressurized medium is modeled by assuming diaphragms to extend from the edges of the repeating unit to the axis of revolution of the cylinder. The diaphragms

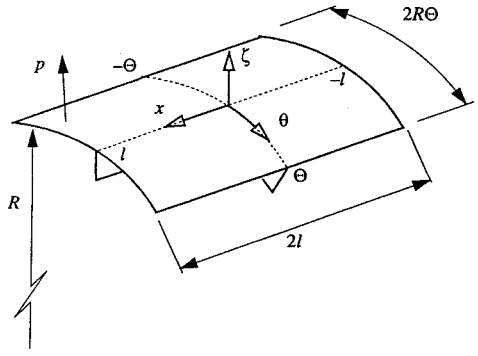

Fig. 1 Structural repeating unit of an orthogonally stiffened cylindrical shell subjected to internal pressure p.

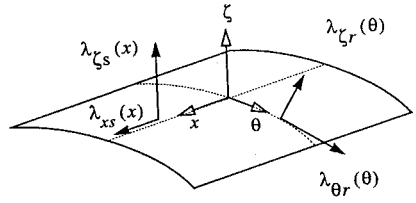

Fig. 2 Distributed line load intensities acting on the inside surface of the shell due to the ring and stringer.

do not resist the deformation of the repeating unit but act to transmit loads normal to the edges of the repeating unit due to internal pressure.

For both the linear and nonlinear response of the repeating unit to internal pressure, we use the Ritz method and the principle of virtual work augmented by Lagrange multipliers to enforce kinematic constraints between the structural components of the repeating unit. The Lagrange multipliers represent the interacting line loads between the stiffeners and the shell. Displacements are separately assumed for the shell, stringer, and ring.

Displacement and Lagrange Multiplier Approximations

The periodic portions of the displacements are represented by truncated Fourier series having fundamental periods in the stringer and ring spacing. The nonperiodic portions of the displacements due to axial stretching are represented by simple terms in x. For the shell, displacements of the middle surface are

$$u(x,\theta) = \frac{q_0 x}{2l} + \sum_{m=1}^{M}\sum_{n=0}^{N} u_{mn}\sin(\alpha_m x)\cos(\beta_n\theta) \tag{1}$$

$$v(x,\theta) = \sum_{m=0}^{M}\sum_{n=1}^{N} v_{mn}\cos(\alpha_m x)\sin(\beta_n\theta) \tag{2}$$

$$w(x,\theta) = \sum_{m=0}^{M}\sum_{n=0}^{N} w_{mn}\cos(\alpha_m x)\cos(\beta_n\theta) \tag{3}$$

in which $\alpha_m = (m\pi/l)$ and $\beta_n = (n\pi/\Theta)$ where m and n are nonnegative integers. The displacements of the centroidal axis of the stringer are

$$\begin{aligned} u_s(x) &= \frac{q_1 x}{2l} + \sum_{m=1}^{M} u_{sm}\sin(\alpha_m x) \\ w_s(x) &= \sum_{m=0}^{M} w_{sm}\cos(\alpha_m x) \end{aligned} \tag{4}$$

Coefficient q_0 in the axial displacement field of the shell and q_1 in the axial displacement field of the stringer represent elongations of each respective element caused by either an axial mechanical load or closed-end pressure vessel effects. The displacements of the reference circle of the ring are

$$\begin{aligned} v_r(\theta) &= \sum_{n=1}^{N} v_{rn}\sin(\beta_n\theta) \\ w_r(\theta) &= \sum_{n=0}^{N} w_{rn}\cos(\beta_n\theta) \end{aligned} \tag{5}$$

The distributions of the interacting loads, or Lagrange multipliers, are taken as

$$\begin{aligned} \lambda_{xs}(x) &= \sum_{m=1}^{M} \lambda_{xsm}\sin(\alpha_m x) \\ \lambda_{\zeta s}(x) &= \sum_{m=1}^{M} \lambda_{\zeta sm}\cos(\alpha_m x) \end{aligned} \tag{6}$$

$$\begin{aligned} \lambda_{\theta r}(\theta) &= \sum_{n=1}^{N} \lambda_{\theta rn}\sin(\beta_n\theta) \\ \lambda_{\zeta r}(\theta) &= \sum_{n=0}^{N} \lambda_{\zeta rn}\cos(\beta_n\theta) \end{aligned} \tag{7}$$

Note that in the stringer interacting normal load the term $\lambda_{\zeta s0}$, which represents a uniformly distributed load, is omitted. Since the stringer as modeled in this analysis is not restrained from the rigid-body motion in the normal direction, the resultant normal load on the stringer must vanish; i.e.,

$$\int_{-l}^{l} \lambda_{\zeta s}(x)\,dx = 0 \tag{8}$$

and this condition requires $\lambda_{\zeta s0}$ to vanish.

Virtual Work

Shell

The generalized strain vector for the shell is

$$\epsilon_{\text{shell}} = [\epsilon_{xx}, \epsilon_{\theta\theta}, \gamma_{x\theta}, \kappa_{xx}, \kappa_{\theta\theta}, \kappa_{x\theta}]^T \tag{9}$$

Assuming the strains are small and rotations are moderately small, the membrane strain-displacement relations are[3]

$$\begin{aligned} \epsilon_{xx} &= \frac{\partial u}{\partial x} + \tfrac{1}{2}\phi_x^2 + \tfrac{1}{2}\phi^2 \\ \epsilon_{\theta\theta} &= \frac{1}{R}\frac{\partial v}{\partial\theta} + \frac{w}{R} + \tfrac{1}{2}\phi_\theta^2 - \tfrac{1}{2}\phi^2 \\ \gamma_{x\theta} &= \frac{\partial v}{\partial x} + \frac{1}{R}\frac{\partial u}{\partial\theta} + \phi_x\phi_\theta \end{aligned} \tag{10}$$

in which ϕ_x is the rotation of the normal around the θ curve, ϕ_θ is the rotation of the normal around the x curve, and ϕ is the rotation around the normal. The rotations are given by

$$\begin{aligned} \phi_x &= -\frac{\partial w}{\partial x} \\ \phi_\theta &= -\frac{1}{R}\frac{\partial w}{\partial\theta} + \frac{v}{R} \\ \phi &= \frac{1}{2}\left(\frac{\partial v}{\partial x} - \frac{1}{R}\frac{\partial u}{\partial\theta}\right) \end{aligned} \tag{11}$$

The change in the normal curvature components in terms of the rotations are

$$\begin{aligned} \kappa_{xx} &= \frac{\partial\phi_x}{\partial x} \\ \kappa_{\theta\theta} &= \frac{1}{R}\frac{\partial\phi_\theta}{\partial\theta} \\ \kappa_{x\theta} &= \frac{\partial\phi_\theta}{\partial x} + \frac{1}{R}\frac{\partial\phi_x}{\partial\theta} + \frac{1}{R}\phi \end{aligned} \tag{12}$$

The Donnell–Mushtari–Vlasov (DMV) approximation, or quasi-shallow shell theory, is obtained by neglecting the rotation about the normal in the strains of Eqs. (10) and (12) and the term v/R in rotation ϕ_θ of Eq. (11). We assume that the contribution of the rotation about the normal to the strains is negligible for the shell but do not assume the DMV approximation initially.

Define the generalized stress vector in terms of the stress resultants and couples of Sanders' theory[3,4] by

$$\sigma_{\text{shell}} = [N_{xx}, N_{\theta\theta}, N_{x\theta}, M_{xx}, M_{\theta\theta}, M_{x\theta}]^T \tag{13}$$

such that the internal virtual work is

$$\delta \mathcal{W}^{\text{int}}_{\text{shell}} = \iint_S \delta \epsilon^T_{\text{shell}} \sigma_{\text{shell}} \, \mathrm{d}S \tag{14}$$

where S denotes the area of the middle surface and $\mathrm{d}S = \mathrm{d}x R \, \mathrm{d}\theta$. Hooke's law for a laminated composite material shell wall is

$$\sigma_{\text{shell}} = H \epsilon_{\text{shell}} \qquad H = \begin{bmatrix} A & B \\ B^T & D \end{bmatrix} \tag{15}$$

in which the 3×3 submatrices A, B, and D are given by classical lamination theory.[5]

The statement of virtual work is

$$\begin{aligned} \delta \mathcal{W}^{\text{int}}_{\text{shell}} = \delta \mathcal{W}^{\text{ext}}_p &+ \int_{-l}^{l} \left\{ \lambda_{xs}(x) \left[\delta u(x,0) - \frac{t}{2} \delta \phi_x(x,0) \right] \right. \\ &\left. + \lambda_{\zeta s}(x) \delta w(x,0) \right\} \mathrm{d}x \\ &+ \int_{-\Theta}^{\Theta} \left\{ \lambda_{\theta r}(\theta) \left[\delta v(0,\theta) - \frac{t}{2} \delta \phi_\theta(0,\theta) \right] \right. \\ &\left. + \lambda_{\zeta r}(\theta) \delta w(0,\theta) \right\} \left(R - \frac{t}{2} \right) \mathrm{d}\theta \end{aligned} \tag{16}$$

for every admissible variation in the shell displacements. For an enclosed volume, the work done by a constant hydrostatic pressure is conservative. (The pressure remains normal to the deformed surface.) The work functional for the constant hydrostatic pressure p is

$$\mathcal{W}^{\text{ext}}_p = \mathcal{W}^{\text{ext}}_{ps} + \mathcal{W}^{\text{ext}}_{pd} \tag{17}$$

where the portion due to work on the shell is

$$\begin{aligned} \mathcal{W}^{\text{ext}}_{ps} = p \iint_S \left\{ (1 + u_x) \left[w + \frac{1}{2R}(w^2 + v^2) \right] \right. \\ \left. + v_y w + \tfrac{1}{3} \det \begin{bmatrix} u & v & w \\ u_x & v_x & w_x \\ u_y & v_y & w_y \end{bmatrix} \right\} \mathrm{d}S \end{aligned} \tag{18}$$

and the portion due to work on the diaphragms at $x = \pm l$ is

$$\mathcal{W}^{\text{ext}}_{pd} = q_0 \left\{ p R^2 \Theta + \frac{p}{6} \int_{-\Theta}^{\Theta} (v_y w - v w_y)\big|_{x=l} R \, \mathrm{d}\theta - Q \right\} \tag{19}$$

In Eqs. (18) and (19) $y = R\theta$, and partial derivatives of the displacements are denoted by a subscript. The axial force Q in Eq. (19) is an additional Lagrange multiplier that accounts for axial load sharing between the stringer and shell.

Stringer

The virtual work statement for the stringer is

$$\begin{aligned} \int_{-l}^{l} [N_{xs} \delta \epsilon_{xs} + M_{xs} \delta \kappa_{xs}] \, \mathrm{d}x = - \int_{-l}^{l} \{ \lambda_{xs}(x) [\delta u_s(x) \\ - e_s \delta w_s'(x)] + \lambda_{\zeta s}(x) \delta w_s(x) \} \, \mathrm{d}x + Q \delta q_1 \end{aligned} \tag{20}$$

in which N_{xs} is the axial force in the stringer, M_{xs} is the bending moment, ϵ_{xs} is the extensional normal strain of the centroidal line, κ_{xs} is the change in curvature of the centroidal line, e_s is the radial distance from the stringer centroid to the contact line along the shell's inside surface, and the prime denotes an ordinary derivative with respect to x. The strain-displacement relations and Hooke's law for the stringer are

$$\epsilon_{xs} = u_s' + \tfrac{1}{2}(w_s')^2 \qquad \kappa_{xs} = - w_s'' \tag{21}$$

$$N_{xs} = (EA)_s \epsilon_{xs} \qquad M_{xs} = (EI)_s \kappa_{xs} \tag{22}$$

Ring

The statement of virtual work for the ring is

$$\begin{aligned} \int_{-\Theta}^{\Theta} [N_{\theta r} \delta \epsilon_{\theta r} + M_{\theta r} \delta \kappa_{\theta r}] R_0 \, \mathrm{d}\theta = - \int_{-\Theta}^{\Theta} \{ \lambda_{\theta r}(\theta) [\delta v_r(\theta) \\ + e_r \delta \phi_r(\theta)] + \lambda_{\zeta r}(\theta) \delta w_r(\theta) \} \left(1 + \frac{e_r}{R_0} \right) R_0 \, \mathrm{d}\theta \end{aligned} \tag{23}$$

in which $N_{\theta r}$ is the circumferential force, $M_{\theta r}$ is the bending moment, $\epsilon_{\theta r}$ is the circumferential normal strain of the centroidal arc, $\kappa_{\theta r}$ is the change in curvature of the reference arc, e_r is the distance from the ring reference arc to the contact line along the shell's inside surface, and R_0 is the radius of the ring's reference arc. The rotation, strain-displacement relations, and Hooke's law for the ring are

$$\phi_r = \frac{1}{R_0}(v_r - \dot{w}_r)$$

$$\epsilon_{\theta r} = \frac{1}{R_0}(\dot{v}_r + w_r) + \tfrac{1}{2}\phi_r^2 \tag{24}$$

$$\kappa_{\theta r} = \frac{1}{R_0}\dot{\phi}_r$$

$$N_{\theta r} = (EA)_r \epsilon_{\theta r} \qquad M_{\theta r} = (EI)_r \kappa_{\theta r} \tag{25}$$

in which the overdot denotes an ordinary derivative with respect to θ.

Displacement Continuity

To maintain continuous deformation between the inside surface of the shell and stiffeners along their lines of contact, the following displacement continuity constraints are imposed:

Along the shell-stringer interface (i.e., $-l \le x \le l$, $\theta = 0$):

$$g_{xs} = u(x,0) - \frac{t}{2}\phi_x(x,0) - [u_s(x) - e_s w_s'(x)] = 0 \tag{26}$$

$$g_{\zeta s} = w(x,0) - w_s(x) = 0 \tag{27}$$

Along the shell-ring interface (i.e., $x = 0$, $-\Theta \le \theta \le \Theta$):

$$g_{\theta r} = v(0,\theta) - \frac{t}{2}\phi_\theta(0,\theta) - [v_r(\theta) + e_r \phi_r(\theta)] = 0 \tag{28}$$

$$g_{\zeta r} = w(0,\theta) - w_r(\theta) = 0 \tag{29}$$

The variational form of these constraints are

$$\begin{aligned} \int_{-l}^{l} [\delta \lambda_{xs} g_{xs} + \delta \lambda_{\zeta s} g_{\zeta s}] \, \mathrm{d}x = 0 \\ \int_{-\Theta}^{\Theta} [\delta \lambda_{\theta r} g_{\theta r} + \delta \lambda_{\zeta r} g_{\zeta r}](R_0 + e_r) \, \mathrm{d}\theta = 0 \end{aligned} \tag{30}$$

The constraint that the axial elongation of the shell at $\theta = 0$ and the stringer are the same is

$$\delta Q [q_1 - q_0] = 0 \tag{31}$$

Satisfying the variational form of constraints, Eqs. (30) and (31), is not sufficient, in general, to satisfying the constraints pointwise, Eqs. (26–29). Since the trigonometric Fourier series functions are linearly independent, and Eq. (31) separately satisfies the polynomial

terms in the axial displacements, the satisfaction of the variational constraints in this analysis does lead to satisfying the constraints pointwise.

Discrete Equations and Their Solution

The discrete displacement vector for the shell is the $(3MN + 2M + 2N + 2) \times 1$ vector

$$\hat{u}_{\text{shell}} = \left[\hat{u}_0^T, \hat{u}_1^T, \ldots, \hat{u}_M^T\right]^T \tag{32}$$

in which the subvectors are

$$\begin{aligned} \hat{u}_0 &= [q_0, w_{00}, v_{01}, w_{01}, \ldots, v_{0N}, w_{0N}]^T \\ \hat{u}_m &= [u_{m0}, w_{m0}, u_{m1}, v_{m1}, w_{m1}, \ldots, u_{mN}, v_{mN}, w_{mN}]^T \end{aligned} \tag{33}$$

where $m = 1, \ldots, M$. The $(2M + 1) \times 1$ discrete displacement vector for the stringer and $(2N + 1) \times 1$ vector for the ring are

$$\begin{aligned} \hat{u}_{\text{str}} &= [q_1, u_{s1}, w_{s1}, \ldots, u_{sM}, w_{sM}]^T \\ \hat{u}_r &= [w_{r0}, v_{r1}, w_{r1}, \ldots, v_{rN}, w_{rN}]^T \end{aligned} \tag{34}$$

in which the term w_{s0} for the stringer has been omitted since it does not deform the stringer and its conjugate resultant in Eq. (8) is equal to zero. This uniform normal displacement component is determined from the condition that the rigid-body displacement of the stringer is the uniform portion of the normal displacement component of the shell at $\theta = 0$; i.e.,

$$\sum_{n=0}^{N} w_{0n} = w_{s0} \tag{35}$$

The discrete vectors of the Lagrange multipliers are

$$\begin{aligned} \hat{\lambda}_{\text{str}} &= [\lambda_{xs1}, \lambda_{\zeta s1}, \ldots, \lambda_{xsM}, \lambda_{\zeta sM}]^T \\ \hat{\lambda}_r &= [\lambda_{\zeta r0}, \lambda_{\theta r1}, \lambda_{\zeta r1}, \ldots, \lambda_{\theta rN}, \lambda_{\zeta rN}]^T \end{aligned} \tag{36}$$

For the nonlinear problem an iterative solution procedure is required. At a fixed value of the pressure p, a sequence of displacements is defined by adding an increment to the previous member of the sequence to determine the next member in the sequence. For a good initial displacement estimate, the sequence converges to the displacement solution of the nonlinear problem. The initial estimate used here is the converged solution at the last pressure load step. The update procedure to determine the increment is based on the modified Newton–Raphson method. To obtain the equations for the Newton–Raphson method, we first derived the virtual work functionals for the shell, stringer, and ring, based on replacing the displacement components by a generic member in their sequence plus an increment. Then the functionals are linearized in the increments. Second, the approximations in Eqs. (1–5) are substituted into the incremented virtual work functionals for the displacements, and similar forms are substituted for their increments. Integration over space is performed after substitution of Eqs. (6) and (7) for the Lagrange multipliers and after substitution for each virtual displacement. [The test space of virtual displacements and the virtual Lagrange multipliers is the same space used for the trial functions in Eqs. (1–7).] This process results in a $3MN+6M+6N+6$ system of equations governing the increment in displacements (indicated by a Δ preceding the displacement subvector symbol) and the Lagrange multipliers. The governing equations are of the form

$$[C] \begin{Bmatrix} \Delta\hat{u}_{\text{shell}} \\ \Delta\hat{u}_{\text{str}} \\ \Delta\hat{u}_r \\ \hat{\lambda}_{\text{str}} \\ \hat{\lambda}_r \\ Q \end{Bmatrix} = \begin{bmatrix} \hat{R}_{\text{shell}}(\hat{u}_{\text{shell}}; p) \\ \hat{R}_{\text{str}}(\hat{u}_{\text{str}}) \\ \hat{R}_r(\hat{u}_r) \\ 0 \\ 0 \\ 0 \end{bmatrix} \tag{37}$$

where the system matrix $[C]$ is given by

$$[C] = \begin{bmatrix} K_{11}(\hat{u}_{\text{shell}}) - pL(\hat{u}_{\text{shell}}) & 0 & 0 & B_{11} & B_{12} & B_{13} \\ 0 & K_{22}(\hat{u}_{\text{str}}) & 0 & B_{21} & 0 & B_{23} \\ 0 & 0 & K_{33}(\hat{u}_r) & 0 & B_{32} & 0 \\ B_{11}^T & B_{21}^T & 0 & 0 & 0 & 0 \\ B_{12}^T & 0 & B_{32}^T & 0 & 0 & 0 \\ B_{13}^T & B_{23}^T & 0 & 0 & 0 & 0 \end{bmatrix} \tag{38}$$

Submatrices K_{11}, K_{22}, and K_{33} are the tangent stiffness matrices for the shell, stringer, and ring, respectively, that are functions of the displacements. The matrix L results from the nonlinear portion of the external work functional for the hydrostatic pressure, Eqs. (17–19). In the modified Newton–Raphson method these matrices K_{11}, K_{22}, and K_{33} and L are only computed for the initial displacement in the sequence and are not updated for each new member in the sequence. The submatrices B_{ij}, $i, j = 1, 2, 3$, in Eq. (38) are determined from the external virtual work terms involving the Lagrange multipliers and the constraint Eqs. (30) and (31). These B_{ij} submatrices are not functions of the displacements. The vector on the right-hand side of Eq. (37) is the residual force vector, which vanishes at equilibrium for the repeating unit. The constraint equations correspond to the last three rows of the partitioned matrix in Eq. (38), and as shown in Eq. (37) these constraints are applied to the increments in the displacements. If the initial estimate of the displacement satisfies these constraint equations and the increments satisfy these same equations, then the final displacement in the sequence will satisfy these same equations. Equation (37) is first solved for the displacements in terms of Lagrange multipliers, and then this solution is substituted into the constraint equations to determine the Lagrange multipliers. Thus, the total solution is obtained.

Numerical Example

Numerical data for the example are $R = 117.5$ in., $2l = 20$ in., $2R\Theta = 5.8$ in., $t = 0.075$ in., $R_0 = 113.72$ in., $e_s = 1.10$ in., $e_r = 3.78$ in., $(EA)_r = 0.592 \times 10^7$ lb, $(EI)_r = 0.269 \times 10^8$ lb-in.^{2}, $(EA)_s = 0.404 \times 10^7$ lb, and $(EI)_s = 0.142 \times 10^8$ lb-in.^{2}, with the shell wall stiffness matrices given by

$$A = \begin{bmatrix} 0.664 & 0.221 & 0 \\ 0.221 & 0.577 & 0 \\ 0 & 0 & 0.221 \end{bmatrix} \times 10^6 \text{ lb/in.} \qquad B = 0$$

$$D = \begin{bmatrix} 262 & 159 & 4.33 \\ 159 & 210 & 4.33 \\ 4.33 & 4.33 & 159 \end{bmatrix} \text{ lb in.}$$

These data were originally used in an example by Wang and Hsu,[6] and the dimensional data are representative of a large transport fuselage. All of the results presented for this example are for an internal pressure $p = 10$ psi. The Fourier series are truncated at $M = N = 16$, unless otherwise indicated. Since $2\Theta = 2.83$ deg, the shell in this example is shallow and the DMV shell theory should be adequate. We found that the numerical results using Sanders theory with the rotation about the normal neglected and the numerical results using DMV theory were essentially the same.

Results and Discussion

Pillowing

Circumferential distributions of the normal displacement w for the shell are shown in Fig. 3 for the linear analysis and in Fig. 4 for the nonlinear analysis. Axial distributions of the normal displacement for the shell are shown in Fig. 5 for the linear analysis and in Fig. 6 for the nonlinear analysis. For reference, the normal displacement for the unstiffened shell, or membrane response, is $w = 0.2287$ in. for the linear analysis and $w = 0.2290$ in. for the

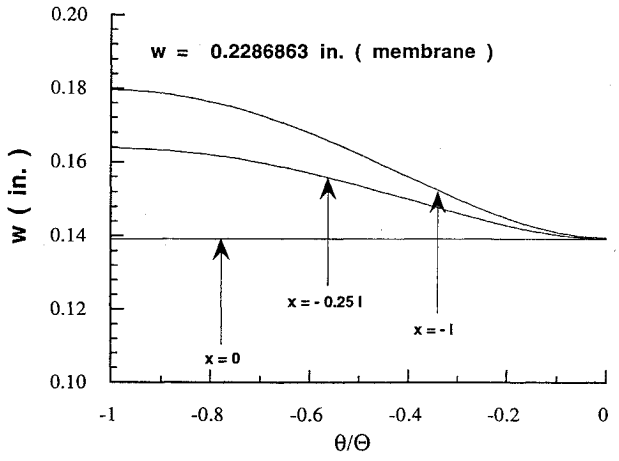

Fig. 3 Circumferential distribution of the shell's normal displacement from the linear analysis.

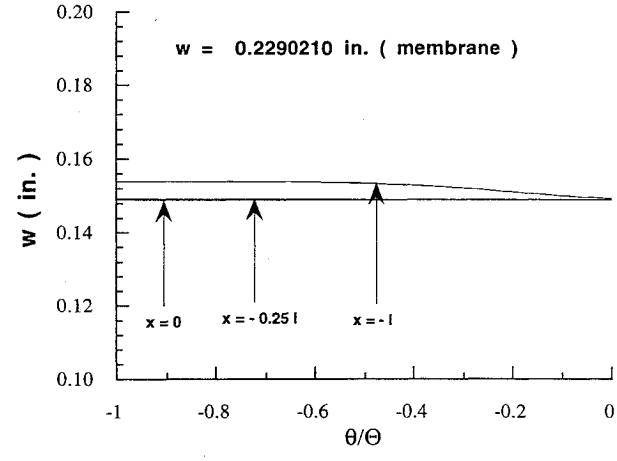

Fig. 4 Circumferential distribution of the shell's normal displacement from the nonlinear analysis.

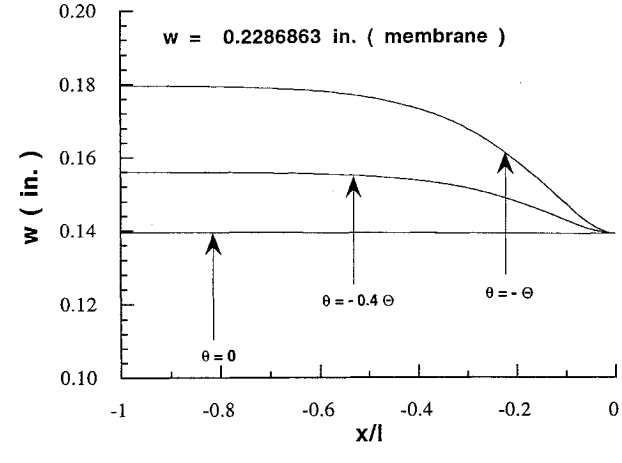

Fig. 5 Axial distribution of the shell's normal displacement from the linear analysis.

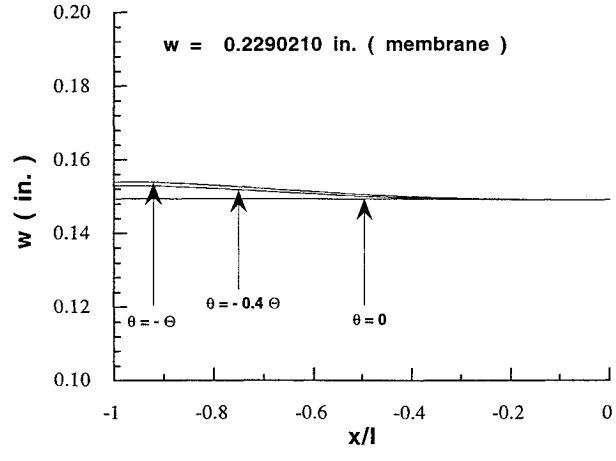

Fig. 6 Axial distribution of the shell's normal displacement from the nonlinear analysis.

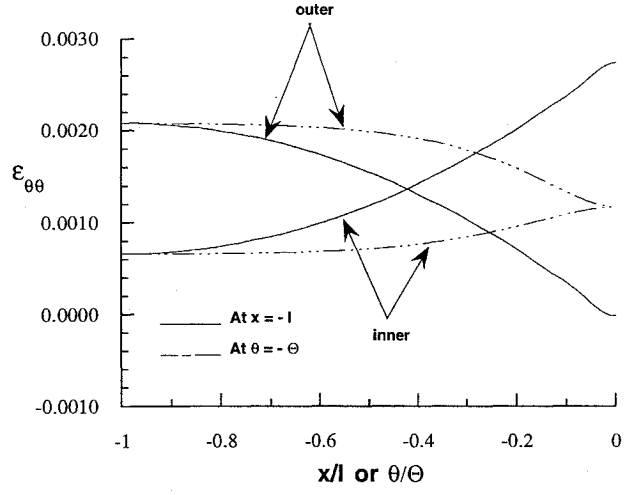

Fig. 7 Circumferential normal strain on the inner and outer shell surfaces from the linear analysis.

nonlinear analysis. The presence of the stiffeners reduces the normal displacements from these membrane values as is shown in these figures. The w distributions shown for the linear analysis compare very well with those presented by Wang and Hsu.[6] (Wang and Hsu's results are limited to linear analysis.) The pillowing effect is much more pronounced for the linear analysis (Figs. 3 and 5) than for the nonlinear analysis (Figs. 4 and 6). The largest normal displacement occurs midway between the stiffeners, and this value for the linear analysis is 0.1796 in., whereas it is 0.1541 in. when geometric nonlinearity is included. The minimum normal displacement occurs at the stiffener intersection, and its value is 0.1392 in. in the linear analysis and 0.1490 in. in the nonlinear analysis. Normal displacements along the stiffeners vary only slightly from their values at the intersection for both analyses. Thus, including geometric nonlinearity in the analysis increases the minimum value of the normal displacement of the shell and decreases its maximum value, which is an indication that pillowing is reduced in the nonlinear response.

The circumferential and axial normal strain distributions on the inner and outer surfaces of the shell also show the reduced pillowing effect in the nonlinear analysis. See Figs. 7–10. The circumferential bending strain (difference in $\epsilon_{\theta\theta}$ between the inner and outer surfaces) is maximum at the stringer midway between the rings (Figs. 7 and 8), and axial bending strain is maximum at the ring midway between the stringers (Figs. 9 and 10). These maximum bending strains are substantially reduced in the geometrically nonlinear response. The values of the ϵ_{xx} and $\epsilon_{\theta\theta}$ strains from the linear analysis (Figs. 7 and 9) compare very well to those presented by Wang and Hsu, except in one respect. The exception is that the circumferential distribution of the axial strain ϵ_{xx} at $x = -l$ (Fig. 9) does not exhibit a decrease in value as the stringer is approached. Wang and Hsu's results, however, show ϵ_{xx} decreasing to nearly zero as the stringer is approached along the circumference. We attempted several changes to the shell displacement approximations and programmed Wang and Hsu's solution, but we could not get any of these attempts to give a solution showing a decrease in the axial normal strain at the stringer.

Bending Boundary Layer

Compare the circumferential normal strain distributions midway between the ring stiffeners ($x = \pm l$) from the linear analysis (Fig. 7) to the nonlinear analysis (Fig. 8). The bending strain magnitudes,

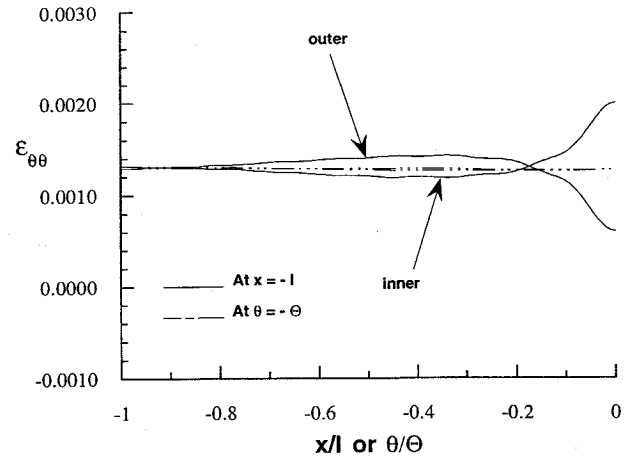

Fig. 8 Circumferential normal strain on the inner and outer shell surfaces from the nonlinear analysis.

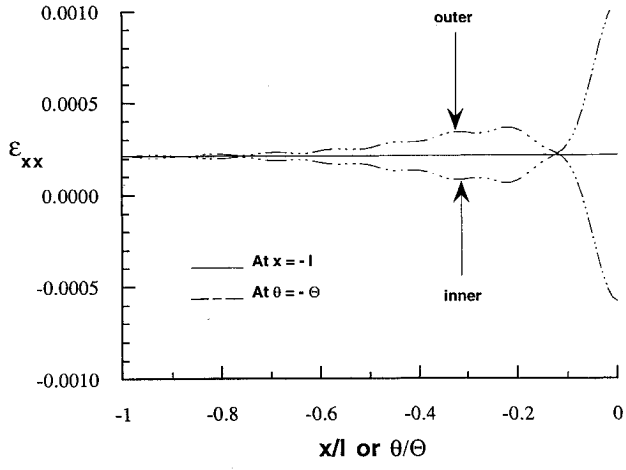

Fig. 9 Axial normal strain on the inner and outer shell surfaces from the linear analysis.

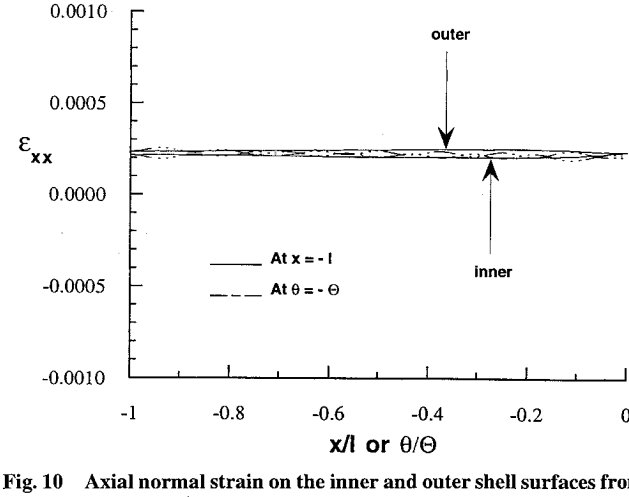

Fig. 10 Axial normal strain on the inner and outer shell surfaces from the nonlinear analysis.

which are differences between the outer and inner normal strain values, are less in the nonlinear response than in the linear response. In the linear analysis the shell exhibits bending over its entire circumference. In nonlinear analysis the shell behaves like a membrane in the central portion with bending confined to a narrow zone, or boundary layer, adjacent to the stringer. Since the bending is confined to a narrow zone near the stringer, the strain gradients are larger in the nonlinear response than in the linear response. These observations are confirmed by plotting the circumferential bending moment $M_{\theta\theta}$ and the circumferential transverse shear resultant Q_θ vs θ/Θ at $x = -l$ as is done in Figs. 11 and 12, respectively. The

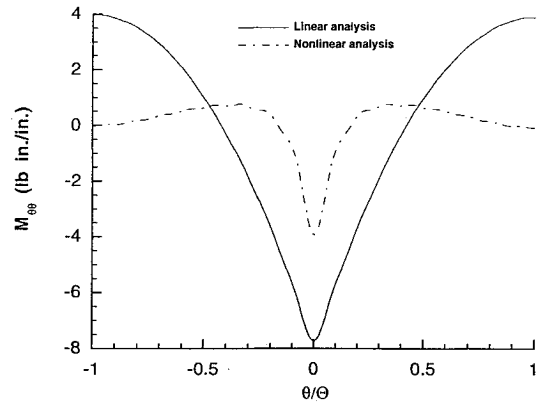

Fig. 11 Distribution of the shell's circumferential bending moment midway between the rings ($x = -l$).

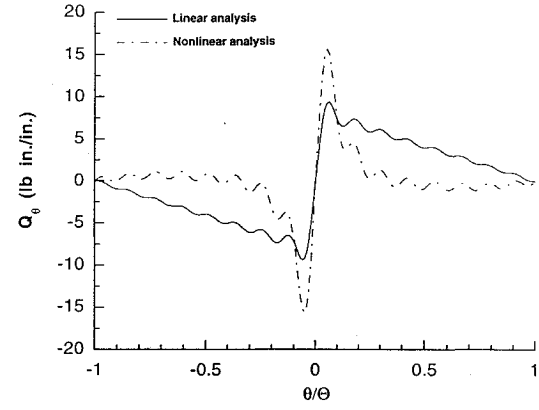

Fig. 12 Distribution of the shell's circumferential transverse shear resultant midway between the rings ($x = -l$).

bending moment magnitude is less in the nonlinear analysis compared with the linear analysis. Moreover, for the nonlinear analysis the bending moment is significantly different from zero only in the boundary layer. This is similar to the distributions of the circumferential strains. By the shell equilibrium, the transverse shear resultant Q_θ is proportional to the derivative (gradient) of bending moment, $\partial M_{\theta\theta}/\partial\theta$. Because the bending moment gradients, or the strain gradients, in the nonlinear analysis are larger than in the linear analysis, the transverse shear resultant has a larger magnitude in the nonlinear analysis than in the linear analysis as is shown in Fig. 12. A larger transverse shear resultant in the nonlinear analysis means that the interlaminar shear stresses are larger in the nonlinear analysis than in the linear analysis. Thus, although pillowing is reduced in the nonlinear response, the confinement of bending to a boundary layer near the stringer results in larger interlaminar shear stresses near the stringer in the nonlinear response than in the linear response. These features of the nonlinear response are consistent with the results found by Boitnott,[7] who examined pressure pillowing of a cylindrical composite panel clamped in a stiff fixture (analogous to rigid stiffeners in the present analysis). Boitnott also showed that the boundary-layer decay length decreased with increasing pressure and decreasing panel thickness.

Interacting Load Distributions

The distributions of the interacting loads between the ring and the shell are shown in Figs. 13 and 14. The distributions of the circumferential component, $\lambda_{\theta r}$, are antisymmetric about the origin, and the component has reduced magnitudes due to the geometrically nonlinear effect. As shown in Fig. 14, the distributions of the normal component of the interacting load, $\lambda_{\zeta r}$, are symmetric about the origin, and the component attains an extremum at the origin, exhibiting a severe gradient there. The negative value of $\lambda_{\zeta r}$ at the origin indicates that the action of the ring is to pull the shell radially inward against the action of the pressure to expand the shell

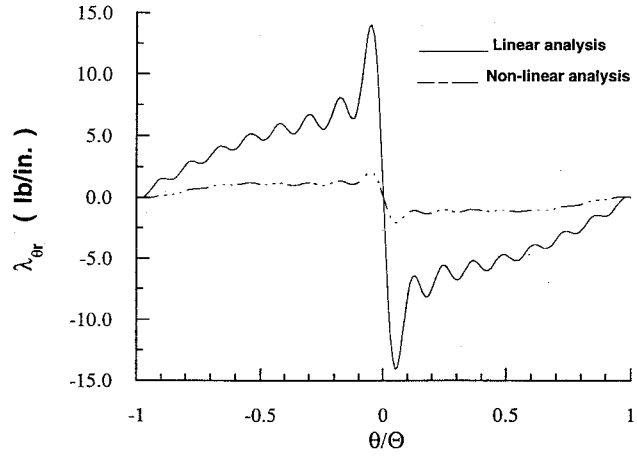

Fig. 13 Tangential component of the line load acting on the shell due to the ring.

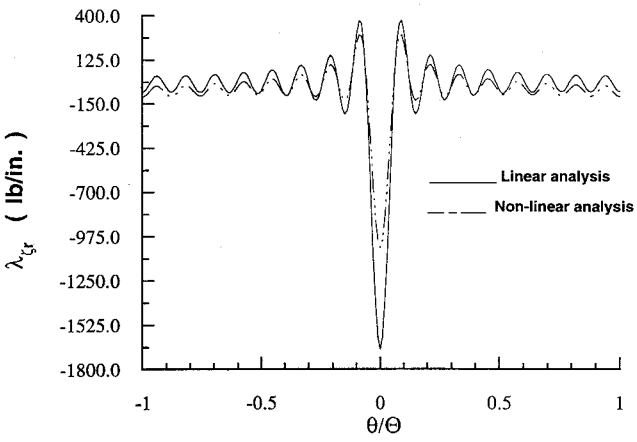

Fig. 14 Normal component of the line load acting on the shell due to the ring.

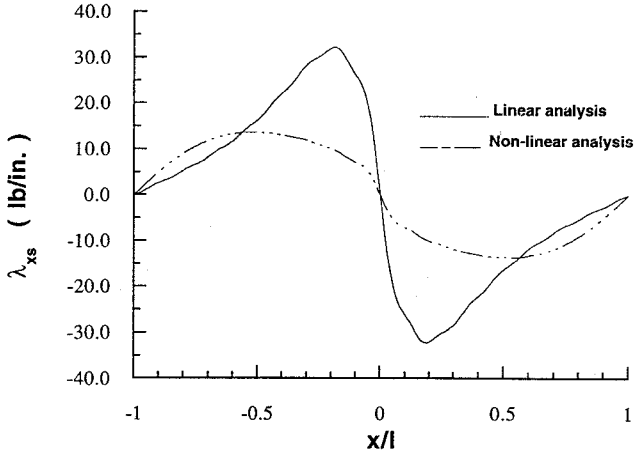

Fig. 15 Tangential component of the line load acting on the shell due to the stringer.

outward. The peak normal load intensity is changed from −1674 lb/in. in the linear analysis to −1045 lb/in. in the nonlinear analysis.

The distributions of the interacting loads between the stringer and the shell are shown in Figs. 15 and 16. The distributions of the tangential component, λ_{xs}, are antisymmetric about the origin, and the component has reduced magnitudes due to the geometrically nonlinear effect as shown in Fig. 15. The distributions of the normal component, $\lambda_{\zeta s}$, are symmetric about the origin. See Fig. 16. The normal component $\lambda_{\zeta s}$ is maximum at the origin and has a steep gradient there. The maximum value of the normal component is reduced from 484.7 lb/in. in the linear analysis to 320.3 lb/in. in the nonlinear analysis. Note that the resultant of this normal component vanishes as a result of Eq. (8).

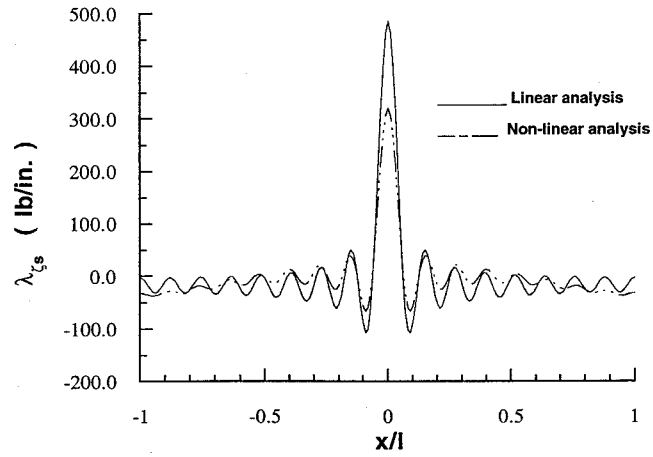

Fig. 16 Normal component of the line load acting on the shell due to the stringer.

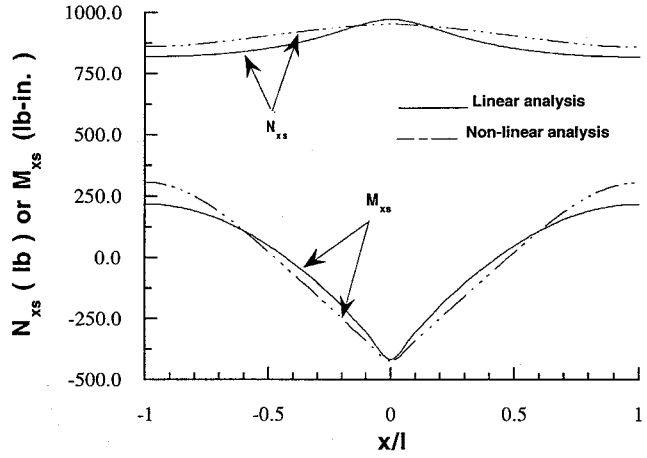

Fig. 17 Stringer axial force and bending moment.

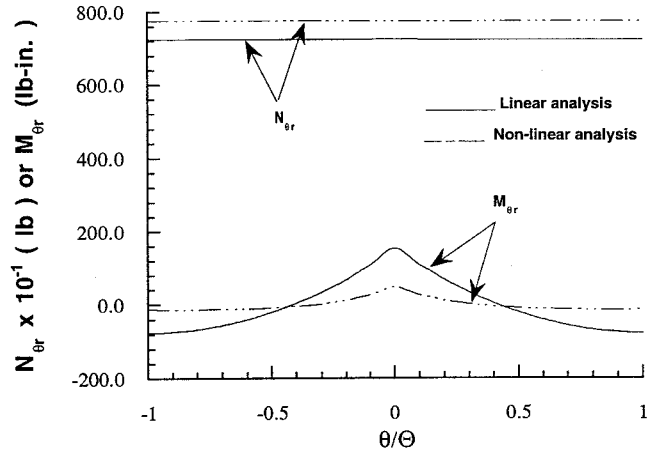

Fig. 18 Ring circumferential force and bending moment.

Stiffener Actions

The distributions of the force and moment resultants in the stiffeners are shown in Figs. 17 and 18. In the linear analysis the total axial load due to the 10 psi pressure is 3407.5 lb [the $pR^2\Theta$ term multiplying q_0 in Eq. (19)], and the portion of this load carried by the stringer is 820.1 lb, or about 24% of the total axial load, according to the value of N_{xs} at $x = \pm l$ shown in Fig. 17. For the nonlinear analysis at 10 psi, the axial load carried by the stringer is increased to about 861.4 lb, or 25.2% of the total axial load. In both the linear and nonlinear analyses, the axial force in the stringer increases slightly from its minimum value midway between the rings to a maximum at the ring location. The bending moment in the ring is reduced by the geometric nonlinearity at the expense of an increase in the value of the circumferential force $N_{\theta r}$ as shown in Fig. 18.

The circumferential force in the ring is nearly uniform and increases from 7242 lb in the linear analysis to 7757 lb in the nonlinear analysis. Thus, the force resultants in the stiffeners increase due to the inclusion of geometric nonlinearity in the analysis.

Singularity at Stiffener Intersection

The results for the interacting normal loads $\lambda_{\zeta s}$ and $\lambda_{\zeta r}$ (Figs. 14 and 16) suggest that they exhibit singular behavior at the stiffener intersection. It is expected that the increased stiffness normal to the structure at the joint, or stiffener intersection, would result in increased normal loads. However, it is likely that the singular behavior at the joint is a mathematical artifact of modeling the contact zone between the shell and stiffeners as a point. The argument for singular behavior is supported by plotting the magnitude of the interacting normal load intensity at the stiffener intersection as M and N increase. The total normal load intensity acting on the shell at the stiffener intersection is denoted by λ_ζ, where $\lambda_\zeta = \lambda_{\zeta r}(0) + \lambda_{\zeta s}(0)$. This value is -1190 lb/in. from the linear analysis and is changed to -725 lb/in. in the nonlinear analysis for $M = N = 16$. A normalized value of λ_ζ is plotted vs increasing M and N values, with $M = N$, in Fig. 19 for the linear analysis and in Fig. 20 for the nonlinear analysis. The normalization factor $\lambda_{\zeta\,\max}$ is simply the value of λ_ζ for the largest values of M and N considered in each analysis. As shown in the figures, λ_ζ is steadily increasing with an increasing number of terms in the truncated Fourier series. Consequently, the series for λ_ζ does not exhibit, in the range of M and N considered, a convergent behavior. In spite of the fact that the normal load intensity at the stiffener intersection is exhibiting singular behavior, the total radial resultant load at the stiffener intersection converges rapidly

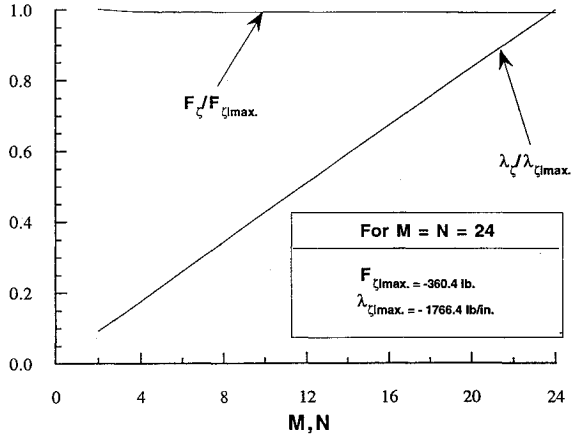

Fig. 19 Normal load intensity λ_ζ and total normal load F_ζ at the stiffener intersection for increasing number of harmonics in the linear analysis.

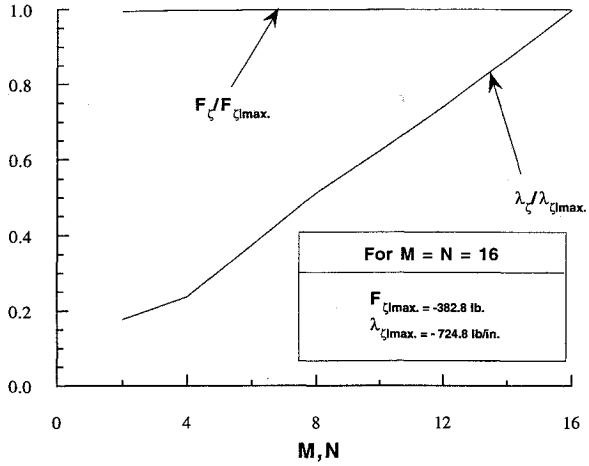

Fig. 20 Normal load intensity λ_ζ and total normal load F_ζ at the stiffener intersection for increasing number of harmonics in the nonlinear analysis.

with increasing values of M and N as shown in Figs. 19 and 20. The total radial resultant plotted in these figures is defined by

$$F_\zeta = \int_{-\Theta}^{\Theta} [\lambda_{\zeta r} \cos\theta - \lambda_{\theta r} \sin\theta](R_0 + e_r)\, d\theta \qquad (39)$$

since the resultant from the stringer vanishes by Eq. (8). From the linear analysis $F_\zeta = -357.5$ lb, and from the nonlinear analysis $F_\zeta = -382.8$ lb. Since the applied radial load due to internal pressure acting on the repeating unit is 1160 lb (= 10 psi × 20 in. × 5.8 in.), the ring resists about 30.8% of this applied load in the linear response, and this percentage is increased to 33% in the nonlinear response. The remaining portion of the applied radial pressure load is carried by the shell.

Concluding Remarks

The spatial distribution of the normal displacements of the cylindrical shell are more uniform, and the bending strains are reduced in the geometrically nonlinear elastic analysis with respect to what is predicted by the linear elastic analysis. That is, pillowing of the skin is reduced by the inclusion of geometric nonlinearity into the analysis. However, in the nonlinear analysis the most severe circumferential bending is confined to a narrow boundary layer adjacent to the stringer midway between the rings, and the interior portion of the shell behaves as a membrane. In the linear analysis the bending occurs over the entire circumference of the shell. The development of the bending boundary layer due to the inclusion of geometric nonlinearity into the analysis causes an increase in the circumferential transverse shear resultant in the shell adjacent to the stringer compared with the linear analysis. Increased interlaminar shear stresses can be expected as a result of the increased transverse shear resultant.

The series for the interacting normal load intensity at the stiffener intersection does not appear to converge in both the linear analysis and in the geometrically nonlinear analysis. The magnitude of the resultant normal load intensity at the stiffener intersection using a truncated Fourier series approximation is decreased by the inclusion of geometric nonlinearity into the analysis. However, a Fourier series for the total radial resultant load carried by the stiffeners, which is resolved at the intersection, exhibits rapid convergence. This total radial resultant carried by the stiffeners is increased slightly by the inclusion of geometric nonlinearity into the analysis. The axial force carried by the stringer due to the closed-end pressure vessel effect is increased in the nonlinear analysis with respect to its value in the linear analysis. Also, the circumferential force carried by the ring is increased in the nonlinear analysis with respect to its value in the linear analysis. Thus, the stiffeners resist an increased portion of the internal pressure load, accompanied by a commensurate decrease in the load carried by the shell, when geometric nonlinearity is included into the analysis.

Acknowledgments

This research is supported by NASA Grant NAG-1-537, and James H. Starnes Jr. of NASA Langley Research Center is the technical monitor. The technical discussions with James Starnes are gratefully acknowledged.

References

[1]Jackson, A. C., Campion, M. C., and Pei, G., "Study of Utilization of Advanced Composites in Fuselage Structures of Large Transports," NASA Contractor Rept. 172404, Contract NAS1-17415, Sept., 1984.

[2]Niu, M. C.-Y., *Airframe Structural Design*, Conmilit Press Ltd., Hong Kong, 1988, pp. 520–526.

[3]Sanders, J. L., "Nonlinear Theories for Thin Shells," *Quarterly of Applied Mathematics*, Vol. 21, No. 1, 1963, pp. 21–36.

[4]Sanders, J. L., "An Improved First-Approximation Theory for Thin Shells," NASA TR R-24, June 1959.

[5]Dong, S. B., Pister, K. S., and Taylor, R. L., "On the Theory of Laminated Anisotropic Shells and Plates," *Journal of the Aerospace Sciences*, Vol. 29, No. 8, 1962, pp. 969–975.

[6]Wang, J. T.-S., and Hsu, T.-H., "Discrete Analysis of Stiffened Composite Cylindrical Shells," *AIAA Journal*, Vol. 23, No. 11, 1985, pp. 1753–1761.

[7]Boitnott, R. L., "Nonlinear Response and Failure Characteristics of an Internally Pressurized Composite Cylindrical Panels," Doctoral Dissertation, Engineering Science and Mechanics Dept., Virginia Polytechnic Inst. and State Univ., Blacksburg, VA, March 1985, pp. 82–97, 104–117.